Organic Electronics 65 (2019) 363–369

Contents lists available at ScienceDirect

Organic Electronics

journal homepage: www.elsevier.com/locate/orgel

Enhanced open-circuit voltages of trifluoromethylated quinoxaline-based polymer solar cells

Sella Kurnia Putri[a,1], Ho Cheol Jin[b,1], Dong Ryeol Whang[c], Joo Hyun Kim[b,*], Dong Wook Chang[a,**]

[a] Department of Industrial Chemistry, Pukyong National University, 48547, Busan, Republic of Korea
[b] Department of Polymer Engineering, Pukyong National University, 48547, Busan, Republic of Korea
[c] Linz Institute for Organic Solar Cells (LIOS)/Institute of Physical Chemistry, Johannes Kepler University Linz, 4040 Linz, Austria

ARTICLE INFO

Keywords:
Quinoxaline
Electron-withdrawing
2,3-Diphenylquinoxaline
Trifluoromethyl
Polymer solar cells

ABSTRACT

Three quinoxaline-based conjugated polymers with donor-π-acceptor configurations have been synthesized by Stille coupling reaction. The electron-donating 2,3-dioctylthienyl- substituted benzodithiophene (BDT) unit was linked to the electron-accepting 2,3-diphenylquinoxaline (DPQ) group through a thiophene bridge, to produce a reference polymer **PTBDT-Qx**. Furthermore, the strong electron-withdrawing trifluoromethyl moieties were introduced at the *para*-position of the phenyl groups in the 2,3-positions of DPQ and 6,7-difluorinated DPQ, to afford **PTBDT-QxCF3** and **PTBDT-FQxCF3**, respectively. Owing to the continuous reduction in their HOMO energy levels with increasing number of electron-withdrawing groups, the open-circuit voltage (V_{oc}) in polymer solar cells (PSCs) shows a gradual improvement in the order of **PTBDT-Qx** < **PTBDT-QxCF3** < **PTBDT-FQxCF3**. The inverted-type PSC based on **PTBDT-FQxCF3** with a configuration of ITO/ZnO/polymer:$PC_{71}BM$/MoO_3/Al provides the best power conversion efficiency of 6.47%, together with a V_{oc} of 0.99 V, a short-circuit current of 10.03 mA/cm^2, and a fill factor of 65.1%.

1. Introduction

Polymer solar cells (PSCs) based on bulk heterojunction (BHJ) structures between polymeric semiconductors and fullerene derivatives have attracted significant attention in the last decades, due to their unique advantages such as low cost, light weight, easy preparation, and outstanding flexibility [1,2]. As a result of continuous efforts to optimize the material design as well as the device fabrication process, the power conversion efficiencies (PCEs) of state-of-the-art PSCs can exceed 10% [3–6]. In order to prepare conjugated polymers appropriate for high-performance PSCs, various studies have attempted to incorporate alternating electron-donating (D) and electron-accepting (A) units along the polymer backbones [7]. In this D-A configuration, the band gap of the polymers can be significantly reduced by the facile formation of an intramolecular charge transfer (ICT) state. Furthermore, important parameters of the D-A polymers including energy levels, band gap and carrier mobility can be easily tuned by the selection and combination of the suitable D and A components [8]. Among various building blocks for constructing the D-A polymers, the quinoxaline (Qx) unit has attracted attention as a promising moiety for the A component, due not only to its strong electron-withdrawing capability but also to other beneficial features such as simple synthesis and a rigid/flat conjugated structure [9–11].

Increasing the open-circuit voltage (V_{oc}) by controlling the energy levels of the conjugated polymers in the active layer of PSCs is currently considered one of the critical tasks for improving the photovoltaic properties of these systems [12]. The V_{oc} of BHJ PSCs is usually determined as the difference between the lowest unoccupied molecular orbital (LUMO) of the electron acceptor and the highest occupied molecular orbital (HOMO) of the electron donor [13]. Therefore, the development of polymeric donors with a low-lying HOMO energy level has become a task of great importance. In this regard, the simple strategy involving the incorporation of electron-withdrawing substituents such as fluorine into the polymer backbone has been intensively investigated [14–18]. Compared to their non-fluorinated counterparts, fluorinated polymers exhibit a substantial reduction in both LUMO and HOMO without significant alteration of their band gaps, which implies an enhanced V_{oc} value when applied in PSCs.

* Corresponding author.
** Corresponding author.
E-mail addresses: jkim@pknu.ac.kr (J.H. Kim), dwchang@pknu.ac.kr (D.W. Chang).
[1] S. K. Putri and H. C. Jin equally contributed to this research.

https://doi.org/10.1016/j.orgel.2018.11.022
Received 17 July 2018; Received in revised form 2 October 2018; Accepted 13 November 2018
Available online 14 November 2018
1566-1199/

Furthermore, the energy levels and photovoltaic properties of D-A type polymers are strongly influenced by the location and concentration of F atoms in their structures [19–21].

Besides fluorine atoms, the introduction of strong electron-withdrawing trifluoromethyl (CF_3) groups in the polymer chains can also lead to a sharp improvement in the V_{oc} of PSCs, through the efficient lowering of the HOMO energy level of the polymers [22,23]. In particular, the CF_3 groups not only possess a higher electron-withdrawing capability than fluorine atoms but also impart unique advantages to the resultant polymers such as high thermal and chemical stability, along with good solubility [24]. The Hammett constants (σ, which are important parameters to determine the electronic characteristics of the substituents) of CF_3 and F at the *para*-position (σ_p) of benzene rings were determined to be 0.54 and 0.06, respectively [25]. For example, the presence of the CF_3 unit either on the electron-withdrawing or electron-donating moiety in D-A polymers can induce the sharp increase in the V_{oc} value of the related PSCs [22,23,26,27].

Herein, we synthesized a series of D-A polymers, in which the electron-donating 2,3-dioctylthienyl substituted-benzodithiophene (BDT) unit was connected to the electron-withdrawing 2,3-diphenylquinoxaline (DPQ) derivatives through a thiophene bridge. Owing to advantageous features including high electron affinity, simple preparation, and facile modification, the DPQ unit was selected as one of basic building blocks for the preparation of reference **PTBDT-Qx** polymer (Fig. 1). It has also been reported that the incorporation of the electron-withdrawing F atoms at the *para*-position of the phenyl rings located in the 2,3-positions of DPQ can efficiently enhance the V_{oc} of the corresponding BHJ PSCs [19,28]. Inspired by these results, strong electron-withdrawing CF_3 moieties (in alternative to fluorine atom) were incorporated at the same positions of DPQ and 6,7-difluorinated DPQ, to afford the target polymers **PTBDT-QxCF3** and **PTBDT-FQxCF3**, respectively (Fig. 1). Owing to the presence of the strong electron-withdrawing moieties, **PTBDT-QxCF3** and **PTBDT-FQxCF3** provide markedly different optical and electrochemical properties compared to the reference **PTBDT-Qx** polymer. In particular, the V_{oc} of inverted-type PSCs based on the three polymers shows a gradual increase in the order of **PTBDT-Qx** < **PTBDT-QxCF3** < **PTBDT-FQxCF3**, with corresponding values of 0.71, 0.91, and 0.99 V, respectively. The increasing trend of V_{oc} is also in good agreement with the progressive increase in the PCEs of PSCs prepared using **PTBDT-Qx**, **PTBDT-QxCF3**, and **PTBDT-FQxCF3** (2.61, 4.61, and 6.47%, respectively).

2. Results and discussion

2.1. Synthesis and characterization

The synthetic approaches used to prepare monomers and polymers are illustrated in Scheme 1. First, the dithiophene-attached benzothiadiazole derivatives of 4,7-di(thiophen-2-yl)benzo[c][1,2,5]thiadiazole (**1**) and 5,6-difluoro-4,7-di(thiophen-2-yl)benzo[c][1,2,5]thiadiazole (**2**) were converted to the associated DPQ units through zinc-mediated reduction followed by a condensation process between the intermediate *o*-diamine and *α*-diketone (Scheme 1). The reaction of **1** with benzyl and 1,2-bis(4-(trifluoromethyl)phenyl)ethane-1,2-dione afforded 2,3-diphenyl-5,8-di(thiophen-2-yl)quinoxaline (**3**) and 5,8-di(thiophen-2-yl)-2,3-bis(4-(trifluoromethyl)phenyl)quinoxaline (**4**), respectively. Moreover, the DPQ possessing two CF_3 groups and two F atoms on its 2,3- and 6,7-positions, respectively, (**5**) was successfully produced by the reaction between **2** and 1,2-bis(4-(trifluoromethyl)phenyl)ethane-1,2-dione. Finally, bromination of **3**, **4**, and **5** using *N*-bromosuccinimide (NBS) yielded the dibrominated DPQ-based monomers **6**, **7**, and **8**, respectively.

In order to prepare conjugated polymers with a typical D-A configuration, the electron-donating 2,3-dioctylthienyl-substituted BDT monomer (**9**) was polymerized with the electron-withdrawing DPQ-based monomers **6**, **7**, and **8** under Stille coupling conditions affording the **PTBDT-Qx**, **PTBDT-QxCF3**, and **PTBDT-FQxCF3** target polymers, respectively. The number average molecular weights (M_n) of **PTBDT-Qx**, **PTBDT-QxCF3**, and **PTBDT-FQxCF3**, recorded by gel permeation chromatography (GPC), were 23.05, 20.21, and 14.61 KDa, respectively, with polydispersity indexes of 2.74, 2.86, and 2.83, respectively. In addition, the three polymers exhibited not only good solubility in common organic solvents such as chloroform, tetrahydrofuran (THF), and toluene, but also high thermal stability. The onset decomposition temperature at 5% weight loss ($T_{d5\%}$) for all polymers could reach up to 415 °C (Fig. 2).

2.2. Optical and electrochemical properties

The UV–Vis absorption spectra of **PTBDT-Qx**, **PTBDT-QxCF3**, and **PTBDT-FQxCF3** measured for films grown on a glass substrate are shown in Fig. 3a, and the corresponding data are summarized in Table 1. Two distinct UV–Vis absorption bands at 400–490 and 500–750 nm were observed for all polymers. The peak at shorter wavelengths (400–490 nm) corresponds to the localized π-π* transition of polymer chains, while the peak in the longer wavelength region (500–750 nm) is related to the ICT between the D and A components in the polymer backbone. Interestingly, the absorption maxima of **PTBDT-QxCF3** and **PTBDT-FQxCF3** at longer wavelengths were shifted to the higher-energies compared to the corresponding peak of **PTBDT-Qx**. These results were attributed to the increased band gap caused by the significant reduction in the HOMO levels of **PTBDT-QxCF3** and **PTBDT-FQxCF3** (*vide infra*). The similar blue-shift in absorption spectra have been also reported for other conjugated polymers possessing electron-withdrawing groups [22,29]. In addition, weak shoulders at ca. 650 nm were observed in the absorption spectra of **PTBDT-QxCF3** and **PTBDT-FQxCF3**, respectively, due to the forced intermolecular aggregation through existing F—F and F—H interactions [30,31]. The optical band gaps of **PTBDT-Qx**, **PTBDT-QxCF3**, and **PTBDT-FQxCF3** determined from the absorption edges were 1.68, 1.69, and 1.71 eV, respectively

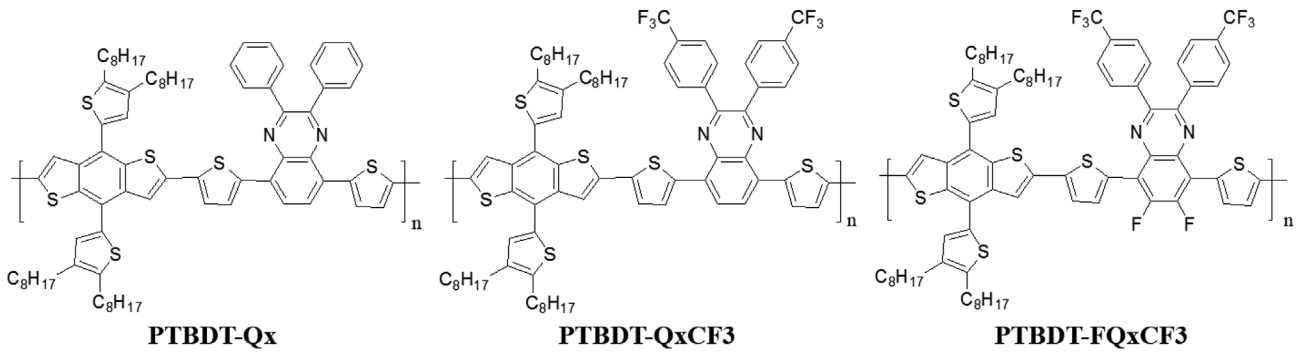

Fig. 1. Chemical structures of **PTBDT-Qx**, **PTBDT-QxCF3**, and **PTBDT-FQxCF3**.

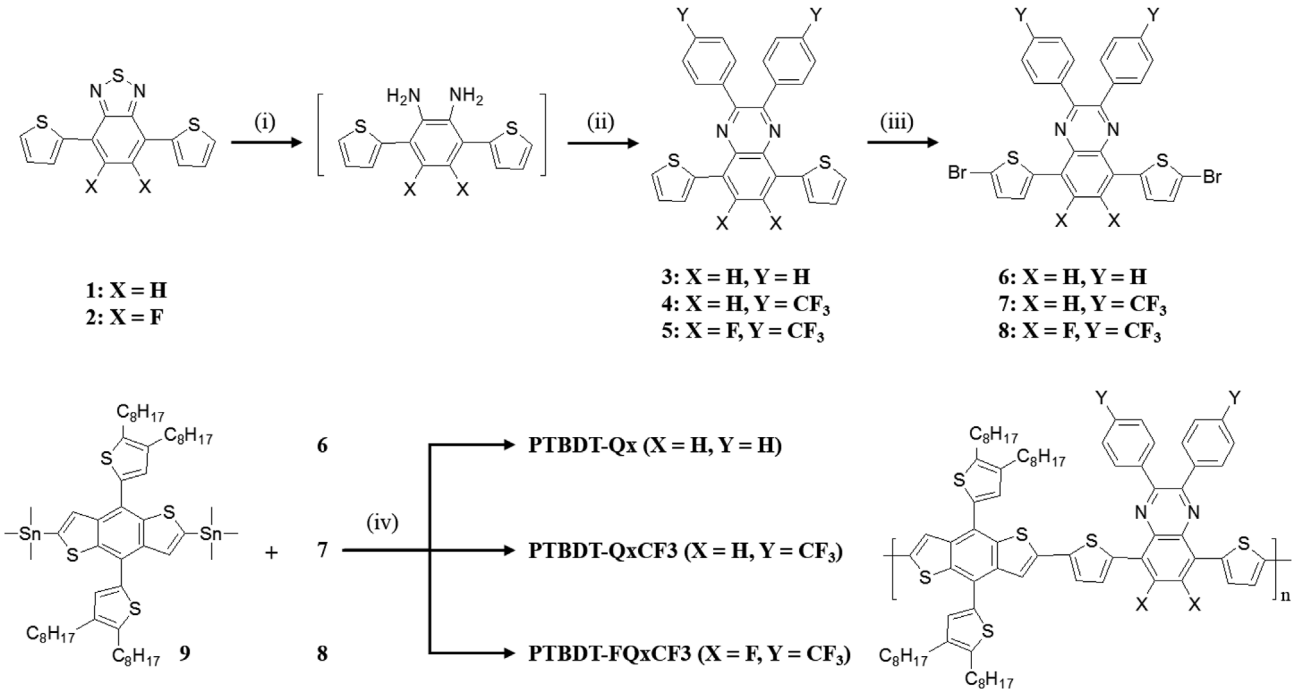

Scheme 1. Synthesis of monomers and polymers: (i) Zn/acetic acid, at 100 °C for 12 h; (ii) *α*-diketone/acetic acid, reflux for 12 h; (iii) NBS, room temperature (RT) overnight; (iv) tetrakis(triphenylphosphine)palladium(0) ($Pd(PPh_3)_4$), at 90 °C for 48 h.

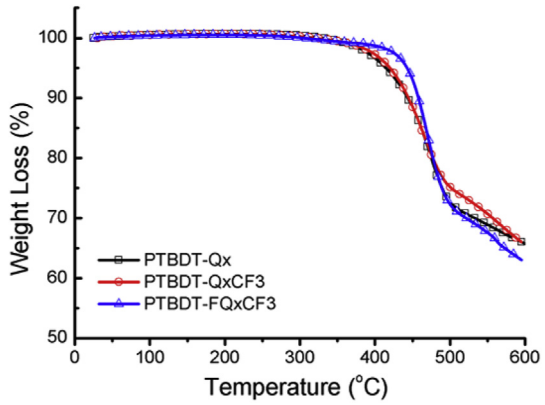

Fig. 2. Thermogravimetric analysis (TGA) thermograms of **PTBDT-Qx**, **PTBDT-QxCF3**, and **PTBDT-FQxCF3** at a heating rate of 10 °C/min under N_2.

(Table 1).

Cyclic voltammetry (CV) measurements were carried out to investigate the energy levels of the polymers, and the results are shown in Fig. 3b. The HOMO energy level of the polymers was calculated from the onset potential of oxidation by assuming the absolute energy level of ferrocene is 4.8 eV below the vacuum level. The HOMO energy levels of **PTBDT-Qx**, **PTBDT-QxCF3**, and **PTBDT-FQxCF3**, calculated from the oxidation onset potential of the cyclic voltammograms with a

Table 1
Summary of optical and electrochemical properties.

	λ_{edge}(nm)[a], E_{gap}^{opt}(eV)[b]	λ_{max}^{film} (nm)[c]	HOMO (eV)[d]	LUMO (eV)[e]
PTBDT-Qx	738, 1.68	441, 622	−5.19	−3.55
PTBDT-QxCF3	733, 1.69	443, 597	−5.47	−3.78
PTBDT-FQxCF3	725, 1.71	441, 601	−5.57	−3.86

[a] Absorption edge of polymer film.
[b] Estimated from the absorption edge.
[c] Maximum absorption wavelength of the film.
[d] Estimated from the oxidation onset potential.
[e] Estimated from the HOMO and the optical band gap.

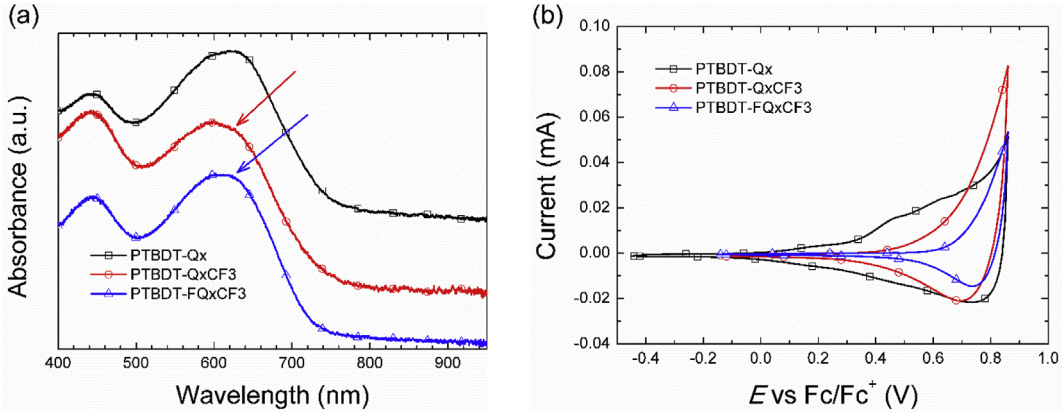

Fig. 3. (a) UV–visible spectra of polymer films on a glass substrate (spectra are offset for clarity) and (b) cyclic voltammograms of polymers.

ferrocene(Fc)/ferrocenium(Fc^+) external standard were −5.19, −5.47, and −5.57 eV, respectively. Upon incorporation of the strong electron-withdrawing CF_3 moieties into the polymer structure, the HOMO energy of **PTBDT-QxCF3** (−5.47 eV) was significantly reduced compared to that of **PTBDT-Qx** (−5.19 eV). A further slight decrease of the HOMO energy (from −5.47 to −5.57 eV) was observed for **PTBDT-FQxCF3**, due to the additional introduction of two F atoms. In addition, the LUMO energy levels of **PTBDT-Qx**, **PTBDT-QxCF3**, and **PTBDT-FQxCF3**, calculated from the difference between HOMO level and the optical band gap, were −3.55, −3.78, and −3.86 eV, respectively. The electrochemical parameters of all polymers are also listed in Table 1. Again, the overall results of the UV–Vis and CV measurements highlight the marked effect of the electron-withdrawing CF_3 unit on the optical and electrochemical properties of DPQ-based polymers.

2.3. Theoretical calculations

To investigate the electronic structures and frontier molecular orbitals of **PTBDT-Qx**, **PTBDT-QxCF3**, and **PTBDT-FQxCF3**, density functional theory (DFT) calculations were performed at the B3LYP/6-31G** level using the Gaussian 09 program [32]. For simplicity, the octyl side chains of the polymers were replaced by short methyl groups, and a two-repeating unit model was adopted in calculations. As shown in Fig. 4, the electron density of the HOMO is almost completely delocalized along the polymer backbone, while that of the LUMO is localized on the electron-withdrawing DPQ units. The calculations also show that the introduction of the strong electron-withdrawing CF_3 substituents significantly lowers both the HOMO and LUMO energy levels of the polymers (from −4.73 and −2.43 eV for **PTBDT-Qx**, respectively, to −4.93 and −2.71 eV for **PTBDT-QxCF3**, respectively). Moreover, the incorporation of two additional fluorine atoms in the DPQ unit to afford **PTBDT-QxCF3** causes further reduction in the HOMO and LUMO energy levels (−4.95 and −2.80 eV). The trends in the theoretical HOMO and LUMO levels of the polymers agree well with determined from the experimental results (Table 1).

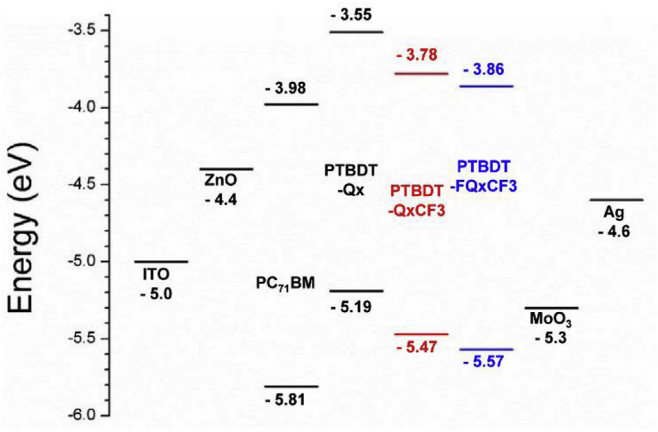

Fig. 5. Energy level diagram of all materials used for the fabrication of inverted-type PSCs.

2.4. Photovoltaic properties

The photovoltaic properties of the polymers were investigated by fabricating inverted-type PSCs with indium tin oxide(ITO)/ZnO (25 nm)/active layer(polymer [6,6]:-Phenyl C_{71} butyric acid methyl ester ($PC_{71}BM$))(80 nm)/MoO_3(10 nm)/Ag(100 nm) structure. The energy levels of all materials used for the device fabrication, shown in Fig. 5, demonstrate the efficient charge separation and charge transport

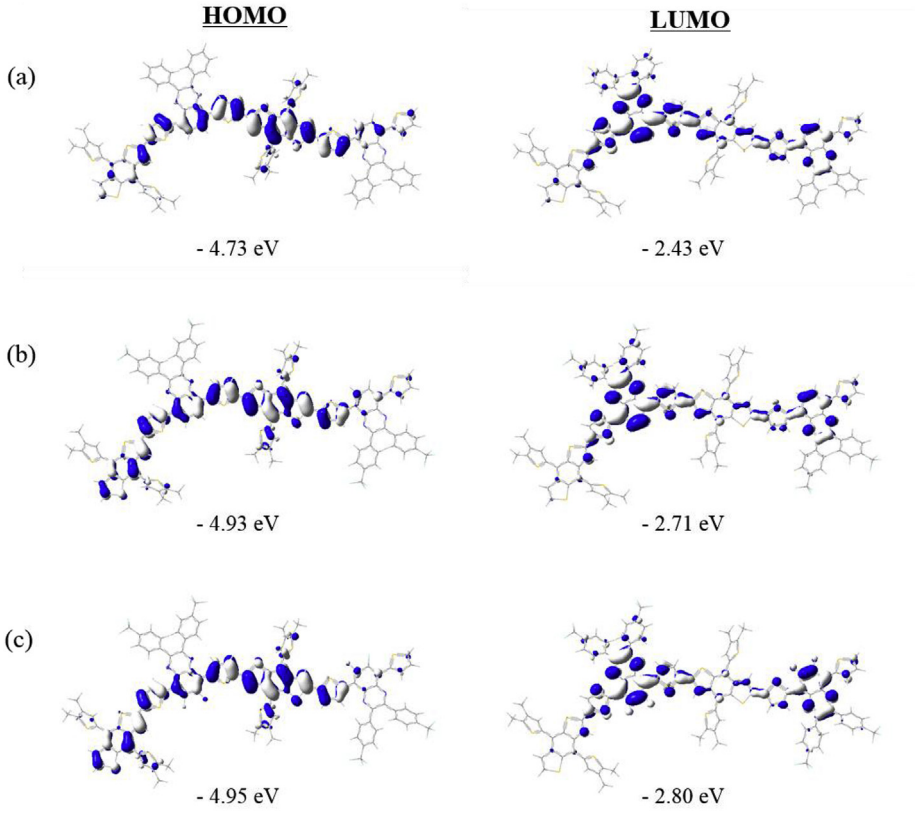

Fig. 4. Frontier molecular orbitals of two-repeating unit models with HOMO and LUMO energy levels calculated at the B3LYP/6-31G** level for (a) **PTBDT-Qx**, (b) **PTBDT-QxCF3**, and (c) **PTBDT-FQxCF3**.

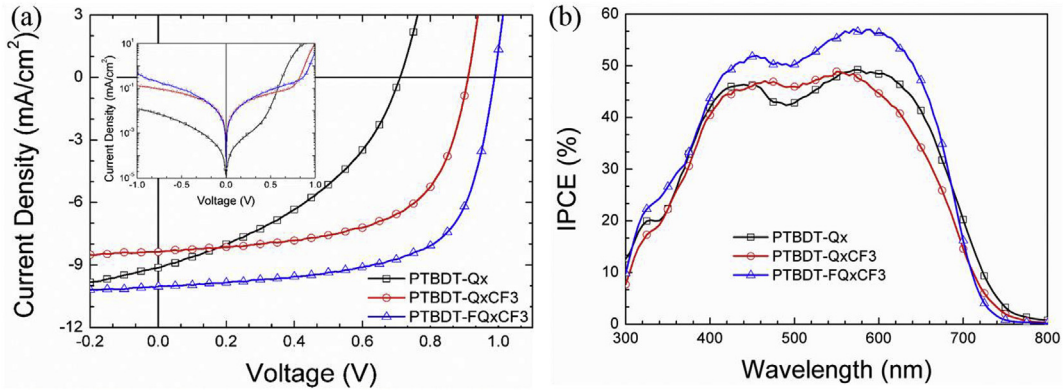

Fig. 6. (a) Current density vs. voltage curves of PSCs with optimum blend ratio of polymeric donors to $PC_{71}BM$, showing the best performances under 1.0 sun condition (inset: under dark conditions); (b) IPCE spectra of PSCs based on **PTBDT-Qx** (squares)**, PTBDT-QxCF3** (circles), and **PTBDT-FQxCF3** (triangles).

Table 2
Best photovoltaic parameters of the PSCs. The average photovoltaic parameters of each device are shown in parentheses.

	J_{sc} (mA/cm^2)	Calculated J_{sc} (mA/cm^2)[a]	V_{oc} (V)	*FF* (%)	*PCE* (%)	R_s (Ω cm^2)[b]
PTBDT-Qx	9.13 (9.05)	9.07	0.71 (0.71)	40.3 (39.7)	2.61 (2.55)	9.61
PTBDT-QxCF3	8.38 (8.07)	8.43	0.91 (0.91)	60.5 (60.9)	4.61 (4.47)	3.36
PTBDT-FQxCF3	10.03 (10.04)	10.11	0.99 (0.99)	65.1 (64.0)	6.47 (6.46)	2.54

[a] Calculated from the IPCE curves.
[b] Series resistance estimated for the corresponding best device.

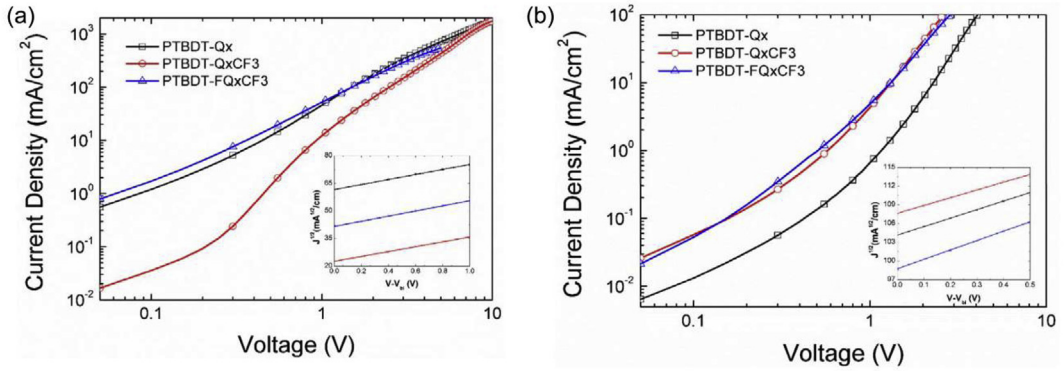

Fig. 7. Current density vs. voltage curves of (a) hole-only (ITO/PEDOT:PSS (35 nm)/polymer:$PC_{71}BM$ (~90 nm)/Au (50 nm)) and (b) electron-only (ITO/Al (20 nm)/polymer:$PC_{71}BM$ (~90 nm)/Al (100 nm)) devices based on **PTBDT-Qx** (squares), **PTBDT-QxCF3** (circles), and **PTBDT-FQxCF3** (triangles) The insets show square root of current density vs. voltage (V)-built-in voltage (V_{bi}), together with fitted lines.

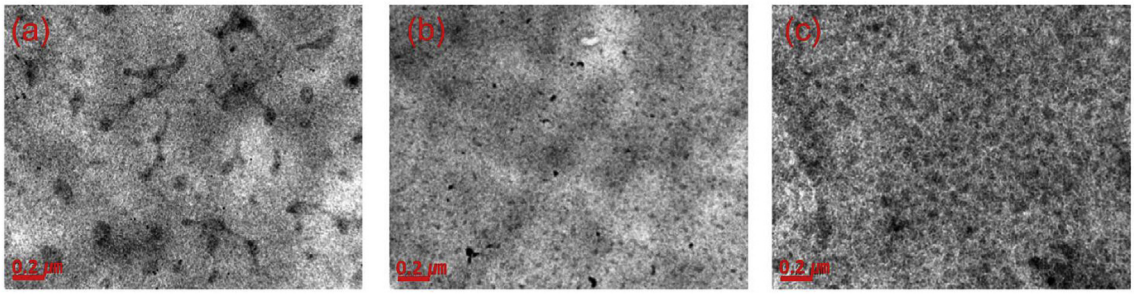

Fig. 8. TEM images of the active layer based on (a) **PTBDT-Qx,** (b) **PTBDT-QxCF3**, and (c) **PTBDT-FQxCF3**.

process in the PSCs. We tested different polymer:$PC_{71}BM$ weight rations (from 3:2 to 3:7), in the active layer of BHJ PSC, and the optimum blend ratios of **PTBDT-Qx**, **PTBDT-QxCF3**, and **PTBDT-FQxCF3** to $PC_{71}BM$ were determined to be 3:3, 3:5, and 3:5, respectively (Table S1).

Fig. 6a shows the optimized current density-voltage (*J-V*) curves of the polymers with the highest PCEs under 1.0 sun condition (the inset shows the curves obtained under dark conditions), and the corresponding device parameters are summarized in Table 2. Interestingly, the PCEs of the polymers gradually increased in the order of **PTBDT-Qx** (2.61%) < **PTBDT-QxCF3** (4.61%) < **PTBDT-FQxCF3** (6.47%). Moreover, the trend in the PCE values is strongly correlated with the similar gradual increase in the V_{oc} of the PSCs. The V_{oc} values measured

for the devices fabricated with **PTBDT-Qx**, **PTBDT-QxCF3**, and **PTBDT-FQxCF3** were 0.71, 0.91, and 0.99 V, respectively. Therefore, the introduction of CF_3 groups at the *para*-position of the phenyl rings located in the 2,3-positions of DPQ moieties in the polymer structure can induce a sharp increase in V_{oc}, of about 28% relative to the original value (from 0.71 V for **PTBDT-Qx** to 0.91 V for **PTBDT-QxCF3**). A similar improvement in the V_{oc} of the corresponding PSCs was obtained upon the incorporation of fluorine atoms at the same positions of DPQ moieties of D-A type polymers [19]. The attachment of fluorine atoms (in addition to the CF_3 groups) on the 6,7-positions of DPQ, affording **PTBDT-FQxCF3** resulted in a further enhancement in V_{oc} up to 0.99 V. The observed changes in the V_{oc} values of PSCs in good agreement with the HOMO levels of the applied polymers (*vide supra*). In addition to the V_{oc} values, the incorporation of the electron-withdrawing groups in the polymer skeleton also improve fill factors (*FFs*) of the devices, and the highest value of 65.1% was achieved for the PSC fabricated with **PTBDT-FQxCF3**. The device based on **PTBDT-FQxCF3** also displayed the highest short-circuit current (J_{sc}) value of 10.03 mA/cm^2, relative to those of the devices based on **PTBDT-Qx** (9.13 mA/cm^2) and **PTBDT-QxCF3** (8.38 mA/cm^2). Overall, these results show that the incorporation of the strong electron-withdrawing CF_3 groups in the polymer backbone is highly beneficial for the photovoltaic properties of PSCs, mainly, through a significant enhancement in the V_{oc} and *FF* values. As shown in Fig. 6b, the incident photon-to-current efficiency (IPCE) curves of all PSCs are well consistent with the absorption behavior of the polymers in the range of 300–800 nm, and provide an adequate explanation for the trend of the J_{sc} values. The calculated J_{sc} values based on incident photon-to-current efficiency (IPCE) spectra showed very good agreement with the J_{sc} data of the devices under 1.0 sun. Furthermore, the series resistance (R_s) of the devices was calculated from the *J-V* curves under dark conditions (inset of Fig. 6a). was calculated. The R_s of the device based on **PTBDT-Qx** (9.61 Ω cm^2) was much larger than the values measured for the devices based on **PTBDT-QxCF3** (3.36 Ω cm^2) and **PTBDT-FQxCF3** (2.54 Ω cm^2) (Table 2). Therefore, the R_s values are gradually decreased with increasing number of electron-withdrawing groups on the DPQ unit, in good agreement with the photovoltaic properties of the devices.

To investigate the charge carrier transport properties of the polymers, we fabricated and tested hole- and electron-only devices with ITO/PEDOT:PSS (35 nm)/polymer:$PC_{71}BM$ (~90 nm)/Au (50 nm) and ITO/Al (50 nm)/polymer:$PC_{71}BM$ (~90 nm)/Al (100 nm) structures, respectively. As shown in Fig. 7a and b, the *J-V* curves of all polymers exhibited space charge-limited current (SCLC) behavior, and could be fitted by the well-known Mott-Gurney law [33]. We calculated the charge mobility using the permittivity of 3.9 for the active layer. The hole mobilities of the devices based on **PTBDT-Qx, PTBDT-QxCF3**, and **PBDT-FQxCF3** were 6.03×10^{-4}, $5.61 \times \times. 10^{-4}$, and 6.29×10^{-4} $cm^2V^{-1}s^{-1}$, respectively. In addition, the electron mobilities of the devices fabricated with **PTBDT-Qx, PTBDT-QxCF3**, and **PBDT-FQxCF3** were $6.00 \times \times. 10^{-4}$, $4.98 \times . 10^{-4}$, and 7.25×10^{-4} $cm^2V^{-1}s^{-1}$, respectively. The hole and electron mobilities of **PBDT-FQxCF3** were higher than those of **PTBDT-Qx** and **PTBDT-QxCF3**. This result is also consistent with the better performances of the **PTBDT-FQxCF3**-based device compared with those of based on **PTBDT-Qx** and **PBDT-FQx**.

The morphologies of the active layers in PSCs were investigated by the transmission electron microscopy (TEM) and the results were shown in Fig. 8. In comparison with the active layer based on **PTBDT-QxCF3** and **PTBDT-FQxCF3**, the active layer based on **PTBDT-Qx** showed relatively larger phase separation and aggregation. In addition, the active layer based on **PTBDT-QxCF3** and **PTBDT-FQxCF3** showed the better bicontinuous interpenetrating networks than that of the active layer based on **PTBDT-Qx**. The best FF of the device based on **PTBDT-QxCF3** and **PTBDT-FQxCF3** were 60.5 and 65.1%, respectively, which are a 50 and 61% increase compared to that of the device based on **PTBDT-Qx**. The morphologies of the active layer support that the FFs of the devices based on **PTBDT-QxCF3 and PTBDT-FQxCF3** are superior to that of the device based on **PTBDT-Qx**. The surface morphologies of the active layers based on **PTBDT-Qx**, **PTBDT-QxCF3**, and **PBDT-FQxCF3**, inspected by tapping-mode atomic force microscopy (AFM) measurements as well, are shown in Fig. S1. The root-mean-square (RMS) of the surfaces of the active layers based on **PTBDT-Qx, PTBDT-QxCF3**, and **PBDT-FQxCF3** were 1.56, 1.70, and 1.60 nm, respectively, indicating that the performances of PSCs are almost independent of the surface morphology and roughness.

3. Conclusions

Three conjugated polymers, in which the electron-donating 2,3-dioctylthienyl-substituted BDT unit was connected to the electron-accepting DPQ derivatives through a thiophene bridge, have been prepared by Stille coupling reaction. To investigate the effects of the strong electron-withdrawing CF_3 substituent on the intrinsic properties of the polymers, CF_3 was systematically incorporated at the para-position of the phenyl groups located in the 2,3-positions of both DPQ, 6,7-difluorinated DPQ, to afford **PTBDT-QxCF3** and **PTBDT-FQxCF3**, respectively. Owing to the strong influences of the CF_3 unit, **PTBDT-QxCF3** and **PTBDT-FQxCF3** exhibit the significant lowering of the HOMO energy levels, which can induce the great enhancement in V_{oc} values of photovoltaic cells. In addition, the incorporation of additional F atom in the presence of CF3 can trigger other positive effects such as enhancement of charge carrier mobility, and formation of better bicontinuous interpenetrating networks in an active layer of device. So, J_{sc} and *FF* of the photovoltaic cells with CF3/F groups can increase sharply. As a result, the PCEs of inverted-type PSCs based on these polymers show a gradual increase in the order of **PTBDT-Qx** < **PTBDT-QxCF3** < **PTBDT-FQxCF3**, with corresponding values of 2.61, 4.61, and 6.47%, respectively. The PCE enhancement can be attributed to the beneficial effect of the CF_3 and CF_3/F substituents incorporated in the polymer backbone, such as the increase in V_{oc} through the lowering HOMO energy levels and the concomitant enhancement in *FF*. Therefore, this study provides meaningful insight into the synthesis and structure-property relationships of conjugated polymers with strong electron-withdrawing CF_3 substituents, which will support their use in various applications such as photovoltaic cells and field-effect transistors.

Acknowledgements

This research was supported by Korea Institute of Energy Technology Evaluation and Planning (KETEP-20174010201460 and 2018201010636A).

Appendix A. Supplementary data

Supplementary data to this article can be found online at https://doi.org/10.1016/j.orgel.2018.11.022.

References

[1] G. Li, R. Zhu, Y. Yang, Polymer solar cells, Nat. Photon. 6 (2012) 153–161.
[2] Y. Huang, E.J. Kramer, A.J. Heeger, G.C. Bazan, Bulk heterojunction solar cells: morphology and performance relationships, Chem. Rev. 114 (2014) 7006–7043.
[3] Y. Liu, J. Zhao, Z. Li, C. Mu, W. Ma, H. Hu, K. Jiang, H. Lin, H. Ade, H. Yan, Aggregation and morphology control enables multiple cases of high-efficiency polymer solar cells, Nat. Commun. 5 (2014).
[4] J. Zhao, Y. Li, G. Yang, K. Jiang, H. Lin, H. Ade, W. Ma, H. Yan, Efficient organic solar cells processed from hydrocarbon solvents, Nature Energy 1 (2016) 15027.
[5] J. You, L. Dou, K. Yoshimura, T. Kato, K. Ohya, T. Moriarty, K. Emery, C.-C. Chen, J. Gao, G. Li, A polymer tandem solar cell with 10.6% power conversion efficiency, Nat. Commun. 4 (2013) 1446.
[6] X. Xu, Z. Li, Z. Wang, K. Li, K. Feng, Q. Peng, 10.20% Efficiency polymer solar cells via employing bilaterally hole-cascade diazaphenanthrobisthiadiazole polymer donors and electron-cascade indene-C70 bisadduct acceptor, Nanomater. Energy 25 (2016) 170–183.
[7] Y.-J. Cheng, S.-H. Yang, C.-S. Hsu, Synthesis of conjugated polymers for organic

solar cell applications, Chem. Rev. 109 (2009) 5868–5923.
[8] Y. Li, Molecular design of photovoltaic materials for polymer solar cells: toward suitable electronic energy levels and broad absorption, Accounts Chem. Res. 45 (2012) 723–733.
[9] J. Chen, Y. Cao, Development of novel conjugated donor polymers for high-efficiency bulk-heterojunction photovoltaic devices, Accounts Chem. Res. 42 (2009) 1709–1718.
[10] H. Yao, L. Ye, H. Zhang, S. Li, S. Zhang, J. Hou, Molecular design of benzodithiophene-based organic photovoltaic materials, Chem. Rev. 116 (2016) 7397–7457.
[11] J. Yuan, J. Ouyang, V. Cimrová, M. Leclerc, A. Najari, Y. Zou, Development of quinoxaline based polymers for photovoltaic applications, J. Mater. Chem. C 5 (2017) 1858–1879.
[12] H.-Y. Chen, J. Hou, S. Zhang, Y. Liang, G. Yang, Y. Yang, L. Yu, Y. Wu, G. Li, Polymer solar cells with enhanced open-circuit voltage and efficiency, Nat. Photon. 3 (2009) 649.
[13] J. Luo, H. Wu, C. He, A. Li, W. Yang, Y. Cao, Enhanced open-circuit voltage in polymer solar cells, Appl. Phys. Lett. 95 (2009) 200.
[14] A.C. Stuart, J.R. Tumbleston, H. Zhou, W. Li, S. Liu, H. Ade, W. You, Fluorine substituents reduce charge recombination and drive structure and morphology development in polymer solar cells, J. Am. Chem. Soc. 135 (2013) 1806–1815.
[15] S.C. Price, A.C. Stuart, L. Yang, H. Zhou, W. You, Fluorine substituted conjugated polymer of medium band gap yields 7% efficiency in polymer− fullerene solar cells, J. Am. Chem. Soc. 133 (2011) 4625–4631.
[16] X.-P. Xu, Y. Li, M.-M. Luo, Q. Peng, Recent progress towards fluorinated copolymers for efficient photovoltaic applications, Chin. Chem. Lett. 27 (2016) 1241–1249.
[17] J. Kim, M.H. Yun, G.-H. Kim, J. Lee, S.M. Lee, S.-J. Ko, Y. Kim, G.K. Dutta, M. Moon, S.Y. Park, Synthesis of PCDTBT-based fluorinated polymers for high open-circuit voltage in organic photovoltaics: towards an understanding of relationships between polymer energy levels engineering and ideal morphology control, ACS Appl. Mater. Interfaces 6 (2014) 7523–7534.
[18] Y. Zhang, J. Zou, C.-C. Cheuh, H.-L. Yip, A.K.-Y. Jen, Significant improved performance of photovoltaic cells made from a partially fluorinated cyclopentadithiophene/benzothiadiazole conjugated polymer, Macromolecules 45 (2012) 5427–5435.
[19] S.K. Putri, Y.H. Kim, D.R. Whang, M.S. Lee, J.H. Kim, D.W. Chang, Step-by-step improvement in photovoltaic properties of fluorinated quinoxaline-based low-band-gap polymers, Org. Electron. 47 (2017) 14–23.
[20] S. Xu, L. Feng, J. Yuan, Z.-G. Zhang, Y. Li, H. Peng, Y. Zou, Hexafluoroquinoxaline based polymer for nonfullerene solar cells reaching 9.4% efficiency, ACS Appl. Mater. Interfaces 9 (2017) 18816–18825.
[21] K.C. Lee, T. Kim, S. Song, Y. Kim, G.K. Dutta, D.S. Kim, J.Y. Kim, C. Yang, Medium bandgap copolymers based on carbazole and quinoxaline exceeding 1.0 V open-circuit voltages, RSC Adv. 6 (2016) 17624–17631.
[22] P. Deng, Z. Wu, K. Cao, Q. Zhang, B. Sun, S.R. Marder, Trifluoromethylated thieno [3, 4-b] thiophene-2-ethyl carboxylate as a building block for conjugated polymers, Polym. Chem. 4 (2013) 5275–5282.
[23] B. Zhang, G. Chen, J. Xu, L. Hu, W. Yang, Feasible energy level tuning in polymer solar cells based on broad band-gap polytriphenylamine derivatives, New J. Chem. 40 (2016) 402–412.
[24] M. Murali, A.D. Rao, P.C. Ramamurthy, New low band gap 2-(4-(trifluoromethyl) phenyl)-1 H-benzo [d] imidazole and benzo [1, 2-c; 4, 5-c′] bis [1, 2, 5] thiadiazole based conjugated polymers for organic photovoltaics, RSC Adv. 4 (2014) 44902–44910.
[25] C. Hansch, A. Leo, R. Taft, A survey of Hammett substituent constants and resonance and field parameters, Chem. Rev. 91 (1991) 165–195.
[26] S.K. Putri, Y.H. Kim, D.R. Whang, J.H. Kim, D.W. Chang, Synthesis of Trifluoromethylated Quinoxaline-Based Polymers for Photovoltaic Applications, Macromolecular rapid communications, 2018, p. 1800260.
[27] J.Y. Shim, T. Kim, J. Kim, J. Kim, I. Kim, J.Y. Kim, H. Suh, Trifluoromethyl benzimidazole-based conjugated polymers with deep HOMO levels for organic photovoltaics, Synth. Met. 205 (2015) 112–120.
[28] C.-P. Chen, Y.-C. Chen, C.-Y. Yu, Increased open circuit voltage in a fluorinated quinoxaline-based alternating conjugated polymer, Polym. Chem. 4 (2013) 1161–1166.
[29] K. Feng, G. Yang, X. Xu, G. Zhang, H. Yan, O. Awartani, L. Ye, H. Ade, Y. Li, Q. Peng, High-performance wide bandgap copolymers using an EDOT modified benzodithiophene donor block with 10.11% efficiency, Advanced Energy Materials 8 (2017) 1602773.
[30] L. Yang, J.R. Tumbleston, H. Zhou, H. Ade, W. You, Disentangling the impact of side chains and fluorine substituents of conjugated donor polymers on the performance of photovoltaic blends, Energy Environ. Sci. 6 (2013) 316–326.
[31] Y. Zhang, S.-C. Chien, K.-S. Chen, H.-L. Yip, Y. Sun, J.A. Davies, F.-C. Chen, A.K.-Y. Jen, Increased open circuit voltage in fluorinated benzothiadiazole-based alternating conjugated polymers, Chem. Commun. 47 (2011) 11026–11028.
[32] M. Frisch, G. Trucks, H.B. Schlegel, G. Scuseria, M. Robb, J. Cheeseman, G. Scalmani, V. Barone, B. Mennucci, G. Petersson, Gaussian 09, Revision a. 02, gaussian, Inc., Wallingford, CT, 2009, p. 200.
[33] A. Bagui, S.S.K. Iyer, Increase in hole mobility in poly (3-hexylthiophene-2, 5-diyl) films annealed under electric field during the solvent drying step, Org. Electron. 15 (2014) 1387–1395.